DR. CECILIA BORASSI (Orcid ID : 0000-0001-6365-363X)

DR. FERNANDO D. MARENGO (Orcid ID : 0000-0002-4372-2092)

RAPID VESICLE REPLENISHMENT AFTER THE IMMEDIATELY RELEASABLE POOL EXOCYTOSIS IS TIGHTLY LINKED TO FAST ENDOCYTOSIS, AND DEPENDS ON BASAL CALCIUM AND CORTICAL ACTIN IN CHROMAFFIN CELLS

Mauricio Montenegro[1], Lucas Bayonés[1], José Moya-Díaz[1], Cecilia Borassi[2], Andrés Martín Toscani[3], Luciana I. Gallo[1] and Fernando D. Marengo[1]

1- Instituto de Fisiología, Biología Molecular y Neurociencias (IFIByNE). CONICET. Departamento de Fisiología y Biología Molecular y Celular. Facultad de Ciencias Exactas y Naturales. Universidad de Buenos Aires. Buenos Aires, Argentina.

2- Fundación Instituto Leloir, Instituto de Investigaciones Bioquímicas de Buenos Aires (IIBBA). CONICET. Buenos Aires, Argentina.

3- Instituto de Química Biológica de la Facultad de Ciencias Exactas y Naturales (IQUIBICEN). CONICET. Departamento de Química Biológica. Facultad de Ciencias Exactas y Naturales. Universidad de Buenos Aires. Buenos Aires, Argentina.

Abbreviated title: IRP replenishment is linked to fast endocytosis

Keywords: actin, calcium, secretion, secretory vesicle, recycling, dynamin

Address for correspondence:

Fernando D. Marengo

Laboratorio de Fisiología y Biología Molecular

Instituto de Fisiología, Biología Molecular y Neurociencias

Facultad de Ciencias Exactas y Naturales - Universidad de Buenos Aires

Ciudad Universitaria

Buenos Aires – Argentina (postal code: 1428)

TEL: +54-11-4576-3368 - FAX: +54-11-4576-3321 - E-mail: fernando@fbmc.fcen.uba.ar

José Moya-Díaz current address: School of Life Sciences, University of Sussex, Brighton BN1 9QG, UK. Mail to: j.moya-diaz@sussex.ac.uk

Andrés Martín Toscani current address: Instituto de Investigaciones Bioquímicas de La Plata (INIBIOLP), Centro Científico Tecnológico – La Plata, Consejo Nacional de Investigaciones Científicas y Técnicas (CONICET), La Plata, Argentina.

ABSTRACT

The maintenance of the secretory response requires a continuous replenishment of releasable vesicles. It was proposed that the immediately releasable pool (IRP) is important in chromaffin cell secretion during action potentials applied at basal physiological frequencies, because of the proximity of IRP vesicles to voltage dependent Ca^{2+} channels. However, previous reports showed that IRP replenishment after depletion is too slow to manage such a situation. In this work we used patch-clamp measurements of membrane capacitance, confocal imaging of F-actin distribution and cytosolic Ca^{2+} measurements with Fura-2 to re-analyze this problem in primary cultures of mouse chromaffin cells. We provide evidence that IRP replenishment has one slow (time constant between 5-10 s) and one rapid component (time constant between 0.5-1.5 s) linked to a dynamin-dependent fast endocytosis. Both, the fast endocytosis and the rapid replenishment component were eliminated when 500 nM Ca^{2+} was added to the internal solution during patch-clamp experiments, but they became dominant and accelerated when the cytosolic Ca^{2+} buffer capacity was increased. In addition, both rapid replenishment and fast endocytosis were retarded when cortical F-actin cytoskeleton was disrupted with cytochalasin D. Finally, in permeabilized chromaffin cells stained with rhodamine-phalloidin, the cortical F-actin density was reduced when the Ca^{2+} concentration was increased in a range of 10–1000 nM. We conclude that low cytosolic Ca^{2+} concentrations, which favor cortical F-actin stabilization, allow the activation of a fast endocytosis mechanism linked to a rapid replenishment component of IRP.

Introduction

The immediately releasable pool (IRP) is a small group of ready releasable vesicles rapidly released by short depolarizations due to their proximity to voltage dependent Ca^{2+} channels (VDCC) (Alvarez & Marengo 2011; Marengo 2005; Voets *et al.* 1999; Horrigan & Bookman 1994). Due to this characteristic, IRP is believed to be particularly sensitive to sharp gradients of Ca^{2+} developed close to VDCC, and therefore it can be important in secretion during action potentials firing at low frequencies where residual Ca^{2+} buildup is supposed to be absent or small (Moya-Diaz *et al.* 2016; Oré & Artalejo 2005).

The replenishment of secretory vesicles pools is essential to maintain chromaffin cell secretion as a function of time. It is classically known, since almost three decades ago, that after strong exocytosis the replenishment of the releasable pools is driven by the mobilization of vesicles from reserve pools (Heinemann *et al.* 1993; Voets *et al.* 1999). Previous studies indicated that replenishment after depletion of IRP is slow (Moser & Neher 1997; Voets *et al.* 1999; Moya-Diaz *et al.* 2016), making difficult the sustained participation of this pool in secretion, even at the lowest physiological frequencies. However, it was described recently that application of a single depolarization, similar in amplitude and temporal course to a native action potential, induces exocytosis of a fraction of IRP (i.e. ETAP, for exocytosis triggered by action potential) which is rapidly replenished with a time constant of 0.7 s (Moya-Diaz *et al.* 2016). The rapid replenishment of ETAP relies on a dynamin-dependent fast membrane retrieval process (referred to as fast endocytosis, with a time constant of approximately 0.5 s), and accounts for the maintenance of synchronous exocytosis during repetitive stimulation at action potential rates below 0.5 Hz. This is in the range of basal frequencies measured in mouse chromaffin cells (Moya-Diaz *et al.* 2016; Wallace *et al.* 2002; de Diego *et al.* 2008; Marcantoni *et al.* 2010; Holman *et al.* 1994). On the other hand, both ETAP and dynamin-dependent fast endocytosis become negligible when action potential rate is increased above 2 Hz (Chan & Smith 2001; Moya-Diaz *et al.* 2016; Moya-Diaz *et al.* 2020). Therefore, it seems that the chromaffin cell invokes different replenishment mechanisms, depending on the stimulation intensity and/or the exocytotic demand.

In this study we further analyzed the mechanisms involved in the whole IRP replenishment and their dependence upon endocytosis, cytosolic Ca^{2+} and cortical actin cytoskeleton. We found that the IRP replenishment exhibits two exponential components: a rapid one with similar kinetics than ETAP recovery; and a slow one, similar to the previously described for whole IRP replenishment.

The increase of cytosolic Ca^{2+} abolishes fast endocytosis, and the rapid replenishment component is lost. In addition, the increase in cytosolic Ca^{2+} buffer capacity correlates with increments in amplitude and rate of endocytosis, together with acceleration of the rapid IRP replenishment. Our results suggest that the high density of cortical F-actin, predominant at low cytosolic Ca^{2+} concentration ($[Ca^{2+}]$), favors a mode of fast endocytosis linked to the rapid replenishment of an IRP fraction which can be released by individual action potentials.

Materials and Methods

Mouse Adrenal Chromaffin Cell Preparation:

All animal procedures were performed under protocols approved by the Consejo Nacional de Investigaciones Científicas y Técnicas (Argentina) and the Facultad de Ciencias Exactas y Naturales, Universidad de Buenos Aires), and are in accordance with the National Institute of Health Guide for the Care and Use of Laboratory Animals (NIH publication 80-23/96), USA. This study was not pre-registered. One hundred fifty female/male 129/sv wild type mice (13-21 days old) were obtained from the Bioterio Central (Facultad de Ciencias Exactas y Naturales, Universidad de Buenos Aires, Argentina). No other inclusion or exclusion criteria were pre-determined for the mice. Animals were housed (6-8 per cage) with ad libitum access to chow and water, under temperature-controlled conditions on a 12 hour light/dark cycle. Animals were sacrificed with intraperitoneal injection of an overdose (500 mg/kg) of tribromoethanol (avertin) to minimize suffering. The avertin solution (20 mg/ml) was prepared by mechanical agitation (4 hours) at room temperature, and kept at 4 °C until use. This anesthesia provokes the total lack of animal reaction to stimuli in less than 3 min after application (0.5 ml/animal), without any sign of suffering or paradoxical side effects. Adrenal glands from two mice were used in each culture (Alvarez *et al.* 2008). In general the animals died because of the anesthesia, but to avoid any possible suffering we always performed cervical dislocation immediately after the end of surgery. Chromaffin cells were isolated and cultured following the procedures described by Perez Bay et al. (Perez Bay *et al.* 2012). Briefly, mechanically isolated adrenal medullas were digested for 25 min in Hanks solution with papain (0.5–1 mg/ml) at 37∘C, and mechanically disrupted in Dulbecco's modified Eagle's medium low glucose, supplemented with 5% fetal calf serum, 5 µl/ml penicillin/streptomycin, 1.3 µl/ml gentamycin, 1 mg/ml bovine serum albumin, and 10 µM cytosine-1-β-D-arabinofuranoside. The cell suspension was filtered through 200 and 50 µm pore meshes, and cultured on poly-L-lysine pretreated coverslips at 37∘C, 95% O_2 – 5% CO_2. The cells were used for experiments between 24-48 hours after culture.

Whole Cell Recording and Membrane Capacitance Measurements:

The patch-clamp setup comprised an inverted microscope (Olympus IX71, Olympus, Japan), a patch-clamp amplifier (EPC10 double patch clamp amplifier USB, Heka Elektronik, Lambrecht,

Germany) and a personal computer. Application of stimulation protocols and acquisition of data were controlled by the Patchmaster® software (Heka, Lambrecht, Germany, RRID:SCR_000034). Chromaffin cells were washed in a standard extracellular solution composed of (mM) 120 NaCl, 20 HEPES, 4 $MgCl_2$, 5 $CaCl_2$, 5 mg/ml d-glucose and 1 μM tetrodotoxin (pH 7.3). In some experiments the external solution was modified as indicated in the text. The cells were maintained in the external solution for at least 10 min before starting with the experiments. The patch-clamp electrodes (3–5 MΩ) were filled with an internal solution containing (mM) 95 Cs D-glutamate, 23 HEPES, 30 CsCl, 8 NaCl, 1 $MgCl_2$, 2 Mg-ATP, 0.3 Li-GTP, and 0.5 Cs- EGTA or 0.5 - 4 Cs-BAPTA (pH 7.2). These solutions were designed to selectively measure voltage-dependent Ca^{2+} currents ($I_{Ca^{2+}}$) and to maximize exocytosis of vesicles tightly coupled to voltage-dependent Ca^{2+} channels, and were used frequently by us to study the exocytosis of IRP (Moya-Diaz *et al.* 2016; Alvarez *et al.* 2008). The micropipettes were coated with dental wax to minimize their stray capacitance and to achieve a better C-fast compensation. The holding potential of -80 mV was not corrected for junction potentials. We considered that the recorded cells were "leaky" and discarded them, when the leak current measured at the holding potential was bigger than −20 pA. We also discarded cells with series resistance bigger than 12 MΩ. The cell capacitance (Cm) was measured continuously during the experiments by application of the sine + dc method (Gillis 1995) implemented through the lock-in extension of Patchmaster, using a sinusoidal voltage (800 Hz, 60 mV peak to peak) added to the holding potential. Application of the sinusoidal voltage was suspended from 10 ms before to 10 ms after the depolarizations applied to stimulate the cells. The synchronous increase in Cm (ΔCm_{exo}), associated with exocytosis, was defined as the difference between the averaged Cm measured in a 50 ms window starting 60 ms after the end of the stimulus, minus the average pre-stimulus Cm, also measured in a 50 ms window. In a similar way, the following decrease in capacitance (ΔCm_{endo}), associated with endocytosis, was calculated as the difference between the averaged Cm measured in a 50 ms window starting 60 ms right after the end of the stimulus, minus the averaged Cm measured 5 s after, also in a 50 ms window (Supplementary Material, Supplementary Figure 1 A). The data were filtered at 3 kHz. The experiments were carried out at room temperature (22–24∘C).

To induce exocytosis of IRP, we employed a single 50 ms square depolarization from the holding potential of -80 to +10 mV. Exocytosis of IRP is triggered by a short depolarization, which provokes specifically the fusion of vesicles located close to VDCC (Horrigan & Bookman 1994), but do not affect other ready releasable vesicles located farther from VDCC. In our laboratory, we

found that in our experimental conditions a square 50 ms depolarization pulse is the best compromise between releasing most of IRP and avoiding the release of extra RRP vesicles (Alvarez *et al.* 2013). We also stimulated the cells with action potential-like stimuli (APls) composed of a 2.5 ms ascendant voltage ramp from -80 to +50 mV, followed by a 2.5 ms descendant ramp that returned to the holding potential. To study the replenishment of IRP or ETAP (exocytosis triggered by action potential), we applied a pair of identical stimuli (single 50 ms square depolarizations or APls, respectively) separated by variable time intervals of 0.2, 0.4, 1, 2, 3, 5, 7, 10, 20 and 40 s respectively (see Figure 1A(i)). The first stimulus depletes the vesicle pool, and the second stimulus of the pair allows us to evaluate the degree of recovery after a certain period. The order of stimuli pairs with the different intervals was organized at random in each experiment using a table of random numbers (Sokal & Rohlf 2009). The different time intervals (in increasing order) were aligned with 10 consecutive numbers of a table column, and then the stimuli pairs with their respective intervals were reordered according the first two digits of the corresponding random numbers. This procedure was repeated in each experiment of every experimental series using different sections of the table. We expressed the degree of replenishment as the ratio between exocytosis evoked by the second stimulus (ΔCm_2) and exocytosis evoked by the first stimulus (ΔCm_1). The ratio $\Delta Cm_2/\Delta Cm_1$ was then plotted against the period between the first and the second stimulus.

Cytosolic Ca^{2+} Measurements:

The experimental setup comprised an upright Olympus microscope BX51WI equipped with a LUMPlanFI/IR 60X/0.90 W (OLYMPUS) objective, and an electron multiplying CCD camera (Andor iXon, Oxford Instruments), controlled by cell-M System Coordinator/cell-Real Time Controller software. The external and internal solutions were similar to those used for electrophysiology, with the exception that the internal solution contained 0.1 mM Fura-2 in salt form. Illumination was achieved with a monochromator device (Polychrome V, Till Photonics) at 340/10 (F_1) and 380/10 nm (F_2). The emitted fluorescence was detected at 510/80 nm (epifluorescence filter block Chroma 79001 ET-Fura-2, Chroma Technology). Fluorescence images of the cells, focused approximately at the equatorial plane, were obtained at both illumination wavelengths during 5 s at 5 Hz (15 ms exposition time). The off-line images were processed with ImageJ free software (https://imagej.nih.gov/ij/). The background fluorescence

(average of three regions of 4.11x1.37 μm) was subtracted from the spatially averaged whole cell fluorescence at each excitation wavelength. Free intracellular Ca^{2+} concentrations were estimated by the formula $[Ca^{2+}]_i = K_d [(R - R_{min})/(R_{máx} - R)] (S_{r2}/S_{b2})$; where $R= F_1/F_2$, S_{r2} and S_{rb} are the emitted fluorescence of Ca^{2+}-free dye and the emitted fluorescence of Ca^{2+}-saturated dye at 380 nm, and a $K_d = 224$ nM for Fura-2/Ca^{2+} (Grynkiewicz *et al.* 1985). R_{max} was obtained at the end of each experiment by breaking the patch pipette to let the external Ca^{2+} diffusing into the cytosol and saturate the indicator. R_{min} was measured in independent cells in presence of internal and external free Ca^{2+} solutions, both with 10 mM BAPTA.

Evaluation of F-actin Cellular Distribution:

The cells were fixed by bath application of 4% paraformaldehyde (v/v) and 4% sucrose (w/v) in phosphate-buffered saline (PBS) for 10 min. After being washed with PBS, cells were incubated in PBS plus tris(hydroxymethil)aminomethano (TRIS) for 10 min. Next, after another wash in PBS the cells were incubated 10 min in rhodamine-phalloidin (1 μM) in PBS (for some preparations we also added DAPI (5 μg/ml)). Finally, the cells were washed 10 times with PBS and then mounted in Mowiol®. Images were obtained with a Zeiss LSM 510 Meta confocal microscope equipped with a Plan-Apochromat 63X/1.4 Oil DIC. Rhodamine-phalloidin was excited at 543 nm and the dye emission was recorded at 560-620 nm. The off-line images were processed with ImageJ free software (https://imagej.nih.gov/ij/). Before fixation, some cells were pretreated with 2 μM cytochalasin D added to the culture medium during 10 min at 37°C to induce the disruption of F-actin (see Figure 7).

To evaluate the effect of cytosolic Ca^{2+} concentration on F-actin distribution the cells were permeabilized during 6 min with 20 μM digitonin and exposed to a solution containing (mM) 139 Cs-glutamate, 33 HEPES (pH 7.2), 30 CsCl, 8 NaCl, 1 $MgCl_2$ 10 Cs-EGTA, 2 Mg-ATP, 0.3 Li-GTP and different free Ca^{2+} concentrations (0.01, 0.1, 1 and 10 μM). The Ca^{2+} concentrations were calculated with the free access software MAXCHELATOR (https://web.stanford.edu/~cpatton/maxc.html) applied for two chelators (ATP and EGTA) and two metals (Ca^{2+} and Mg^{2+}), at 25°C and 0.173 N ionic force. The cells were fixed and labeled with rhodamine-phalloidin as explained previously.

Materials

Bovine serum albumin (CAT No. 05470-25G), poly-L-lysine (CAT No. P8920-100ML), cytosine-1-beta-D-arabinofuranoside (CAT No. C6645-25MG), papain (CAT No. P4762-100MG), Mg ATP (CAT No. A9187-100MG), Li GTP (CAT No. G5884-25MG), EGTA (CAT No. E4378-10G), BAPTA (CAT No. A4926-1G) and cytochalasin D (CAT No. C8273) were obtained from Sigma (St Louis, MO, USA); Dulbecco's modified Eagle's medium (CAT No. 10567-014), gentamycin (CAT No. 15750078) and penicillin/streptomycin (CAT No. 15140122) from Gibco (Carlsbad, CA, USA); fetal calf serum from Natocor (Córdoba, Argentina, CAT No. SFB500ml); tetrodotoxin citrate from Alomone Labs (Jerusalem, Israel, CAT No. T-550); Fura-2 from Invitrogen (Carlsbad, CA, USA, CAT No. F6799); rhodamine-phalloidin from Thermo Fisher (Waltham, MA, USA, CAT No. R415); and the monoclonal anti-dynamin antibody (BD Biosciences, San Jose, CA, EEUU, CAT No. 610246, RRID:AB_397641).

Data Analysis and Statistics

To estimate the cortical actin density as represented in Supplementary Figure 3B (ii) we measured the fluorescence associated with rhodamine-phalloidin at four rectangular areas (4.11 x 1.37 µm) equidistant each other in the cell border (Supplementary Material, Supplementary Figure 1B), and averaged after background subtraction. Finally, for each culture, the individual cell values were divided by the averaged fluorescence intensity of control cells not treated with digitonin (4 cultures with 8-21 control cells each), and averaged.

Data are expressed as mean values ± standard error of measurements obtained in different cells (one measurement per cell, and one cell per petry dish). For every experimental condition, the data were always obtained from several cell cultures. The number of cell cultures used in every experimental condition and for each measured variable is represented in Supplementary Table 3. No blinding and no sample calculation were performed in this study. The sample sizes were adjusted according the variability in every experimental series. No test for outliers was performed. Statistical analysis was carried out using the statistical package of Sigma Plot 11.0 (Systat Software, RRID:SCR_003210). We used the Student's "t" test for comparisons between two groups of independent data samples. One way ANOVA was used for multiple independent data samples, and Bonferroni test for comparisons between groups. If samples did not pass the

normality test (Shapiro-Wilk), we used the Mann-Whitney rank sum test or Kruskal–Wallis one way analysis of variance on ranks, respectively. In the latter case, we used the Dunn´s test for comparison between groups. To fit endocytosis records, or replenishment curves of IRP or ETAP, we used the nonlinear curve-fitting option in Origin Pro 8 (Microcal Software, RRID:SCR_002815). The comparison between fittings with different number of exponential components was performed with a Fisher test which considers the residual sum of square errors and the degree of freedom of each model (Origin® statistical package).

<center>**Results**</center>

Fast Endocytosis and Vesicle Replenishment after Immediately Releasable Pool (IRP) Exocytosis:

To measure IRP exocytosis, we reproduced the standard conditions used in our previous publications (Alvarez *et al.* 2008; Moya-Diaz *et al.* 2016). To maximize exocytosis of vesicles tightly coupled to voltage-dependent Ca^{2+} channels, external and internal solutions contained 5 mM Ca^{2+} and 0.5 mM EGTA respectively (Moya-Diaz *et al.* 2016) (see Materials and Methods). Exocytosis was induced by a 50 ms square depolarization pulse (from -80 to +10 mV) which completely releases IRP in our chromaffin cell preparation (Alvarez *et al.* 2013). To evaluate IRP replenishment after depletion, the experimental protocol involved application of several pairs of 50 ms square depolarizations separated by variable time periods and organized at random in each cell (see Figure 1A(i) and Materials and Methods). Figure 1A (ii) and (iii) illustrate typical records of Ca^{2+} current ($I_{Ca^{2+}}$) and cell membrane capacitance (ΔCm) obtained in response to application of the paired protocol with 5 s interval between stimuli. There was no difference between the amplitude of $I_{Ca^{2+}}$ evoked by the first and second depolarization pulse of the pair (163±19 and 157±18 pA respectively; n=28). To standardize the estimations of $I_{Ca^{2+}}$ and exocytosis (ΔCm_{exo}) along the work we always computed the measurements obtained on the first depolarization of the first pair of pulses applied in each cell (see the example in Fig. 1A). $I_{Ca^{2+}}$ and ΔCm_{exo} induced by this stimulus averaged 163±19 pA and 21±2 fF respectively (n=28). This ΔCm_{exo} is similar to previous estimations of IRP obtained by us in the same conditions, and falls within the range of values reported by other authors in chromaffin cells (Alvarez *et al.* 2008; Alvarez & Marengo 2011; Horrigan & Bookman 1994; Voets *et al.* 1999). In 85% of the cells, exocytosis of IRP was followed by a fast decrease in Cm (Fig. 1A(iii)), which resembles to fast endocytosis described previously by us and other authors (Moya-Diaz *et al.* 2016; Chan & Smith 2001; Wu & Wu 2014). As explained before for $I_{Ca^{2+}}$ and ΔCm_{exo}, to standardize the estimations of endocytosis (ΔCm_{endo}) we always measured the decay in Cm after the first depolarization of the first pair of pulses applied in each cell. In addition, to ensure completion of this endocytotic process, we evaluated ΔCm_{endo} only in cells for which the first pair of pulses was separated at least by 5 s (see Methods). After all these considerations, only three experiments showed a non-measurable decay in Cm and were included in the statistics with a value equal to zero, and ΔCm_{endo} averaged 8.5±1.6 fF (n=21). We used the ratio between endocytosis and exocytosis amplitudes (endo/exo) as an index of

endocytotic compensation efficiency. In our standard conditions we obtained endo/exo = 0.45±0.06 (n=21). Finally, the Cm decay associated with endocytosis was fitted in each experiment to a single exponential function (we excluded experiments with high basal noise and those with $\Delta Cm_{endo} \leq 3$ fF), obtaining an average time constant (τ_{endo}) of 1.23±0.18 s (n=12; an example is shown in Fig. 1A(iii), white line).

In a previous paper we have concluded that IRP is replenished with a kinetics that follows a single exponential function with a time constant (τ_R) of approximately 7 s (Moya-Diaz *et al.* 2016). However, in that work the shortest interval applied between stimuli was 2 s, so we could have potentially lost a faster component. Furthermore, in the same work we found that a small group of vesicles, released by a single action potential-like stimulus and named as ETAP (for exocytosis triggered by action potential), recovers ten times faster, with a τ_R of 0.7 s. Therefore, it is possible that the kinetics of IRP replenishment presents actually two components, a rapid and a slow one. In order to reevaluate the kinetics of IRP replenishment, in this work we applied an extended protocol from our previous work by including short (0.2, 0.4 and 1 s) as well as long (2, 3, 5, 7, 10, 20 and 40 s) intervals between stimuli. Figure 1B shows the average results obtained for IRP replenishment from these experiments. The experimental points of Figure 1B were fitted initially to a single exponential growing function, obtaining a time constant τ_R of 3.28±0.68 s (R^2= 0.966, reduced chi square=1.054; Supplementary Material, Supplementary Figure 1C and Supplementary Table 1). However, this fitting ignored the average experimental points obtained at 0.2, 20 and 40 s intervals. Furthermore, this time constant is approximately two times faster than the one obtained previously by us for IRP replenishment (Moya-Diaz *et al.* 2016), probably because of the inclusion of the shorter intervals. On the other hand, when the experimental curve was fitted to a double growing exponential function (Figure 1B), the quality of the fitting improved significantly (R^2= 0.996, reduced Chi Square=0.122, p<0.05 (Fisher test), Supplementary Table 1) and the fitting line connected every point. The time constant of the slower component (τ_{R2} = 10.42 s) was close to the one previously obtained by us for IRP, and the rapid time constant (τ_{R1} = 1.07 s) was very similar to the one previously described for the replenishment of ETAP (Moya-Diaz *et al.* 2016).

Effects of cytosolic [Ca^{2+}] on fast endocytosis and IRP replenishment

The results obtained in the previous section indicate that IRP replenishment is better represented by two growing exponential components. To study if these components might reflect two different processes, we analyzed IRP replenishment dependency with cytosolic [Ca^{2+}]. Our speculation was that different molecular processes probably have different Ca^{2+} dependencies. Cytosolic Ca^{2+} affects diverse processes associated with vesicle replenishment. For example, transport of vesicles through cytoskeleton, transference of vesicles to the ready releasable pool, priming and endocytosis are affected by [Ca^{2+}] (Rose *et al.* 2001; Voets *et al.* 1999; Sorensen 2004; Wu & Wu 2014).

First, we repeated the same experimental conditions of the previous section but adding 500 nM free Ca^{2+} to the electrode internal solution. The free [Ca^{2+}] was calculated with the free access software MAXCHELATOR (https://web.stanford.edu/ ~cpatton/maxc.html) applied for two chelators (ATP and EGTA) and two metals (Ca^{2+} and Mg^{2+}), at 25°C and 0.173 N ionic force. Figure 2A shows a typical record of cellular capacitance during application of a pair of 50 ms square depolarizations separated by 5 s in this high [Ca^{2+}] condition. Table 1 summarizes the averaged values of these experiments in comparison with the control condition represented in Figure 1. Fast endocytosis, measured in absolute values as ΔCm_{endo}, as well as in relative values with respect to the previous exocytosis (endo/exo), was basically abolished at high [Ca^{2+}]. Surprisingly ΔCm_{exo} was not modified by the increase in basal [Ca^{2+}], although this behavior can be explained by the significant reduction in I_{Ca2+} (Table 1).

Figure 2B represents the average IRP replenishment (expressed as $\Delta Cm_2/\Delta Cm_1$) curve obtained in presence of 500 nM cytosolic Ca^{2+}. The average experimental points were fitted to a single exponential growing function, obtaining a time constant τ_R of 5.22 s (R^2=0.973, reduced Chi Square=0.587). The fitting line crosses close to every experimental point, and application of a double exponential function did not improve the fitting appreciably (R^2=0.975, reduced Chi Square = 0.526, p>0.328 (Fisher test, Supplementary Table 1)). We also fitted individual experiments (i.e. each replenishment curve for every individual cell) and obtained an almost identical time constant of replenishment (averaged τ_R = 5.28±1.30 s, n=7, for examples see Supplementary Figure 1D (i) and (ii)). In conclusion, the increase of basal cytosolic Ca^{2+} abolished fast endocytosis and reduced IRP replenishment to only one relatively slow component. The speed of this replenishment process is approximately the double of the slow component and five times slower than the rapid component measured in the control condition. Although we

cannot assign this replenishment to any particular process, our results show that it is not directly related to fast endocytosis. Therefore, it is clearly different to the rapid replenishment process associated with exocytosis induced by a single action potential (Moya-Diaz *et al.* 2016).

The second experimental approach used to evaluate the effect of cytosolic $[Ca^{2+}]$ on IRP replenishment and fast endocytosis consisted in enhancing the cytosolic Ca^{2+} buffering capacity by addition of increasing concentrations of BAPTA to the internal solution. Increasing BAPTA concentration from 0.5 to 4 mM did not provoke a significant change in the amplitude of exocytosis (Figures 3A and 3C). Even though ΔCm_{exo} showed some decreasing tendency, it did not reach statistical significance, which may be due to a compensatory effect caused by the significant enhancement of $I_{Ca^{2+}}$ at high BAPTA concentrations (Figure 3B). Importantly, the augment of BAPTA concentration significantly increased endocytosis amplitude and endo/exo ratio (Figures 3A, 3D and 3E). In fact, at 4 mM BAPTA the parameter endo/exo approached 1, turning from a non-compensatory to a fully compensatory endocytosis. Moreover, endocytosis was markedly accelerated at high BAPTA concentrations, with significantly reduced τ_{endo} values (Figure 3F).

The results described above indicate that chromaffin cell fast endocytosis was increased and accelerated in presence of a high Ca^{2+} buffer capacity. However, this effect might be indirectly caused as a consequence of a local Ca^{2+} increase produced by the increment of $I_{Ca^{2+}}$ at high BAPTA concentrations. To evaluate this possibility, we measured the changes in membrane capacitance induced by 50 ms depolarizations in presence of 0.5 mM intracellular BAPTA but with 10 mM Ca^{2+} in the extracellular solution, in an attempt to obtain a higher $I_{Ca^{2+}}$, similar to the one measured with 4 mM intracellular BAPTA. This increase in extracellular $[Ca^{2+}]$ provoked significant augments in $I_{Ca^{2+}}$ and in exocytosis with respect to the experiments performed at 5 mM extracellular $[Ca^{2+}]$ (Supplementary Figures 2 A-C). It is important to note that the $I_{Ca^{2+}}$ obtained at 10 mM Ca^{2+} was very similar to the one represented in Figure 3B for 4 mM BAPTA. Nevertheless, endocytosis was not augmented nor accelerated in response to the increase in extracellular $[Ca^{2+}]$ with concomitant increase in $I_{Ca^{2+}}$ (Supplementary Figures 2 D-F). On the contrary, high external $[Ca^{2+}]$ seemed to be associated with decreases in size and speed of endocytosis, although these tendencies were not significant.

The results represented in Figure 3 and Supplementary Figure 2 indicate that it is the increase in Ca^{2+} buffer capacity itself with concomitant reduction in cytosolic $[Ca^{2+}]$, and not the increase in

I_{Ca2+}, what provokes the magnification of endocytosis. Additionally, IRP replenishment was also accelerated with the increase in BAPTA concentration. Figure 4 shows average replenishment curves at 0.5, 1, 2 and 4 mM BAPTA. Every curve was fitted well by a single exponential function, and application of a double exponential did not significantly improve these fittings (see all fitting parameters and statistical values associated with the Fisher test in Supplementary Table 1). The replenishment obtained in the experiments performed at 0.5 mM cytosolic BAPTA (Figure 4A) followed an exponential behavior with similar kinetics to the fast component fitted at 0.5 mM EGTA (please compare τ_R of Figure 4A with τ_{R1} of Figure 1B). More importantly, the time constant of replenishment τ_R was reduced approximately four times when BAPTA was increased from 0.5 to 4 mM (Figure 4, A-D). We also fitted individual experiments. As an example, Figure 5A (i) and (ii) show replenishment curves obtained from 2 single cells dialyzed with 0.5 and 4 mM BAPTA, respectively. Figure 5B summarizes the averaged values of time constants τ_R obtained from these individual fittings performed on every BAPTA concentration tested. This additional analysis confirms the significant reduction of the replenishment time constant τ_R (i.e. the acceleration of the replenishment process) at high BAPTA concentrations.

Interestingly, the estimations of τ_{endo} and τ_R in 4 mM BAPTA condition were both very similar to the those previously determined by us for ETAP (Moya-Diaz *et al.* 2016). In this previous work, we found that fast endocytosis and rapid ETAP replenishment were significantly inhibited by dialysis of a monoclonal antibody against dynamin (antiDyn) through the patch micropipette. We and other authors reported previously the efficiency of this antibody to block the actions of dynamin (Gonzalez-Jamett *et al.* 2010; Moya-Diaz *et al.* 2016). Fast endocytosis and internalization of a transferrin-conjugate and an anti-dopamine-b hydroxylase antibody in mouse chromaffin cells were blocked by antiDyn (Moya-Diaz *et al.* 2016). Dynamin is a protein involved in the final steps of various modes of endocytosis (Artalejo *et al.* 2002; Watanabe *et al.* 2013; Wu *et al.* 2014). The interpretation of those results was that fast endocytosis was dynamin dependent, and it was a necessary process for the development of rapid replenishment (i.e. if fast endocytosis is inhibited or retarded we expect to see a similar effect on the rapid replenishment). Therefore, we next evaluated the effect of antiDyn on these two processes when cells were measured in presence of 4 mM intracellular BAPTA. In agreement with our previous results, we found that antiDyn (dialyzed during 5 min after whole-cell establishment) provoked a significant deceleration of fast endocytosis (see individual examples represented in Figure 6A). Also, replenishment was decelerated by antiDyn. Figure 6B represents averaged replenishment curves and Figure 6C shows

two independent examples of replenishment curves obtained in individual cells, in control and in antiDyn condition respectively. The different parameters measured in these experiments are summarized in Table 2, where it is shown that AntiDyn significantly increased τ_{endo} and τ_R. In other words, inhibition of dynamin decelerated both fast endocytosis and replenishment.

In summary, the results of this section illustrate that different experimental strategies that modify intracellular $[Ca^{2+}]$ provoke changes in fast endocytosis and IRP replenishment: the increase in intracellular $[Ca^{2+}]$ inhibits fast endocytosis and abolishes the rapid component of replenishment, while increase in cytosolic Ca^{2+} buffer capacity (which implies a decrease in intracellular $[Ca^{2+}]$) potentiates and accelerates endocytosis and also accelerates replenishment. Finally, the results also show that both processes depend on dynamin.

Effect of cytosolic $[Ca^{2+}]$ on cortical F-actin

The previous section showed that cytosolic $[Ca^{2+}]$ modulates both fast endocytosis and replenishment associated with IRP exocytosis. Ca^{2+} can potentially modulate endocytosis and vesicle replenishment through different mechanisms (Wu & Wu 2014; Chan *et al.* 2003; Elhamdani *et al.* 2006; Heinemann *et al.* 1993; Voets *et al.* 1999; Trifaro *et al.* 2008). In this section we evaluated the effect of cytosolic $[Ca^{2+}]$ on cortical F-actin because: (i) actin cytoskeleton remodeling and severing is finely regulated by Ca^{2+} (Lueck *et al.* 2000; Rodriguez Del Castillo *et al.* 1990; Kumar *et al.* 2004); and (ii) there is accumulated evidence for the pivotal role of cortical F-actin in the regulation of exocytosis, endocytosis and vesicle trafficking to plasma membrane in chromaffin and other cells (Boulant *et al.* 2011; Watanabe *et al.* 2013; Rose *et al.* 2001; Doreian *et al.* 2008; Shin *et al.* 2018).

As a first step, we estimated cytosolic $[Ca^{2+}]$ with Fura-2 (0.1 mM) in three different buffering conditions used in our previous experiments: 0.5 mM EGTA, 0.5 BAPTA and 4 mM BAPTA added to the internal solution (see Materials and Methods for solution compositions). Supplementary Figure 3A shows examples of experimental records obtained with 0.5 and 4 mM BAPTA. When averaged, the estimated $[Ca^{2+}]$ at 0.5 mM BAPTA and at 0.5 mM EGTA were very similar, 60±14 nM (n=18) and 69±26 nM, (n=12, not shown) respectively; but 4 mM BAPTA reduced significantly the cytosolic $[Ca^{2+}]$ to 18±7 nM (n=13; p<0.05).

To evaluate the effects of cytosolic Ca^{2+} on cellular F-actin we exposed digitonin-permeabilized cells to either 0.01, 0.1, 1 or 10 μM Ca^{2+} (see Materials and Methods), fixed the cells, and evaluated the cortical F-actin density using confocal microscopy and rhodamine-phalloidin as a fluorescent F-actin marker. Supplementary Figure 3B (i) shows individual examples of cell images obtained under these four conditions. As expected, F-actin was mostly concentrated in the cortical region of the cell. More importantly, F-actin density decreased as $[Ca^{2+}]$ was augmented. The cortical F-actin density was evaluated in four regions of interest in each cell (Supplementary Figure 1B), and the summary of these results is represented in Supplementary Figure 3B (ii). There was a highly significant decrease of cortical F-actin density with the increment of $[Ca^{2+}]$. Moreover, it is particularly remarkable that the different cytosolic $[Ca^{2+}]$ estimated or fixed in our previous experiments (see red arrows at 20, 60 and 500 nM Ca^{2+}) are localized in the steeper region of the curve.

Importance of cortical F-actin on fast endocytosis and rapid IRP replenishment

The experiments explained in the previous section indicate that low cytosolic $[Ca^{2+}]$ promotes a high F-actin density at the cell cortical region. Therefore, cortical F-actin density might be a potential factor contributing to the observed fast endocytosis and rapid IRP replenishment measured at 4 mM BAPTA. The rationale of this hypothesis is based on previous observations by others: particularly cortical F-actin dynamics promotes endocytosis (Boulant *et al.* 2011; Watanabe *et al.* 2013), vesicle transport (Rose *et al.* 2001; Li *et al.* 2018) and "kiss-and-run" mode of vesicle fusion/fission which is supposedly associated with fast endocytosis and rapid recycling (Doreian *et al.* 2008; Elhamdani *et al.* 2006). Based on our hypothesis, we expect that a pharmacological induction of actin depolymerization should revert in part the acceleration of endocytosis and replenishment promoted by high BAPTA concentration. To depolymerize F-actin we pretreated cells with 2 μM cytochalasin D (Cyto D) during 10 min at 37°C. Figure 7A shows examples of cells labeled with the F-actin fluorescent marker rhodamine-phalloidin. While in control conditions F-actin was mainly distributed as a continuous ring in the cortical region of the cells, Cyto D treatment provoked a totally different pattern with discontinued F-actin distribution in the cortex as well as in the inner cytoplasmatic regions. We quantified the cortical F-actin reported by rhodamine-phalloidin fluorescence in a 1 μm wide ring area surrounding the border of the cell. We found that the relative fluorescence of the cell cortex, with respect to the whole cell

fluorescence, was significantly reduced by Cyto D treatment (1.50±0.04 (n=11) vs 1.15±0.04 (n=9), p<0.05).

We evaluated the effect of Cyto D treatment on endocytosis and replenishment in cells dialyzed with 4 mM BAPTA. Figure 7B shows two typical capacitance records obtained under control and Cyto D condition. This treatment reduced both exocytosis and endocytosis amplitudes, but endo/exo ratio was not modified and endocytosis completely compensated the previous exocytosis in both conditions (see Table 3 and Figure 7B). Importantly, the rate of endocytosis was significantly reduced by Cyto D treatment (see the increase in τ_{endo} values in Figure 7B and Table 3). In addition, average replenishment curves (Figures 7C (i) and (ii)), as well as replenishment curves obtained for individual cells (see Supplementary Figures 4A and B for examples, and Table 3 for averaged values), show that τ_R increased significantly after Cyto D treatment, implying that replenishment was also decelerated.

Importance of cortical F-actin on fast endocytosis and rapid ETAP replenishment

We have shown before (Moya-Díaz et al, 2016) that fast endocytosis and replenishment associated with ETAP are partially inhibited and retarded by application of dynamin blockers. These result were confirmed in this work by application of antiDyn and 80 µM dynasore (Supplementary Figure 5, A and B; τ_{endo} were 1.49±0.12 s (n=5) and 1.26±0.39 s (n=7) for antiDyn and dynasore, respectively, and τ_R for dynasore was 2.38±0.68 s (n=7)). We now wondered if F-actin might also contribute to fast endocytosis and rapid replenishment coupled to ETAP (Moya-Diaz *et al.* 2016). Figure 8A shows the depolarization template (i.e APls, see Methods) used to stimulate cells (i), and examples of recordings of $I_{Ca^{2+}}$ (ii) and capacitance (iii) obtained in two independent experiments performed under control condition (left) and after Cyto D pretreatment (right). Cyto D did not modify either $I_{Ca^{2+}}$, exocytosis, endocytosis amplitude nor endo/exo ratio (see Table 3). Endocytosis nearly compensated previous exocytosis in both conditions (ratios endo/exo were close to 1). However, Cyto D treatment significantly decelerated endocytosis (see τ_{endo} for control and Cyto D for the examples of individual experiments in Figure 8A (iii)) and replenishment (see τ_R for the average replenishment curves in Figures 8B (i) and (ii), and in the examples of individual experiments in the Supplementary Figure 4C and D). Averages of τ_{endo} and τ_R obtained from individual experiments are represented in Table 3.

In conclusion, the results of the two last sections support the hypothesis that cortical F-actin contributes to the regulation of dynamin-dependent fast endocytosis and the associated rapid replenishment after IRP exocytosis.

Discussion

In this work we found that IRP is replenished after depletion with two components: a slow one, in agreement with previous reports (Moser & Neher 1997; Moya-Diaz *et al.* 2016); and a rapid one, as recently described by us for ETAP (Moya-Diaz *et al.* 2016). To our knowledge, two components of replenishment were previously described for the ready releasable pool (Voets *et al.* 1999; Gomis *et al.* 1999; Chan *et al.* 2005), but not for IRP. This solves the apparent paradox that has arisen from our previous work, which described that ETAP is a fraction of IRP but recovers ten times faster than the whole IRP (Moya-Diaz *et al.* 2016). This rapid component is markedly potentiated at low cytosolic [Ca^{2+}], and this behavior can be explained, at least in part, by the presence of a highly dense cortical F-actin.

Rapid Replenishment is linked to Fast Endocytosis

Exocytosis of IRP in our standard conditions is followed by a fast endocytosis that compensates about half of the previous membrane capacitance increase (Figure 1). Every experimental intervention that modifies fast endocytosis also changes the rapid replenishment of IRP in the same direction. First, inhibition of dynamin decelerates both fast endocytosis and rapid replenishment (Figure 6), in agreement with our previous results obtained for ETAP (Moya-Diaz *et al.* 2016). Second, 500 nM cytosolic Ca^{2+} abolished rapid replenishment and fast endocytosis; and inversely, these two processes were potentiated and accelerated as Ca^{2+} buffer capacity was augmented by increasing cytosolic BAPTA concentration (Figures 2-5). Third, rapid replenishment and fast endocytosis were decelerated by cortical F-actin disruption (Figures 7 and 8). Taken together, these results strongly suggest that rapid replenishment is linked to fast endocytosis. Notably, the time constant of rapid replenishment shows similar values to the time constant of endocytosis in every experimental condition performed in this work. This parallel behavior of rapid replenishment and fast endocytosis velocities adds additional support to the interdependence between both variables. These results are in agreement with our previous report showing that rapid ETAP replenishment is tightly linked to a dynamin-dependent fast endocytosis (Moya-Diaz *et al.* 2016), and support the presence of a novel fast recycling mechanism of IRP vesicles in chromaffin cells.

Rapid Replenishment and Fast Endocytosis are Potentiated at Low Cytosolic Ca^{2+}

To study the effect of low cytosolic $[Ca^{2+}]$ on fast endocytosis and IRP replenishment we applied BAPTA at different concentrations. The cells with BAPTA lacked the slow component of replenishment. Considering BAPTA fast Ca^{2+} binding kinetics, it seems that this phenomenon could be related to a process influenced by sharp Ca^{2+} gradients that developed close to VDCC during I_{Ca2+} activation. One possibility is that the slow replenishment might be associated with vesicle trafficking towards the exocytotic site, influenced by local Ca^{2+} (Becherer *et al.* 2003). Another possibility is that the presence of BAPTA selects for fusion a subpopulation of vesicles that is even closer to VDCC than the rest of IRP vesicles, and that this subpopulation would be associated with rapid replenishment. This second hypothesis might be related to ETAP (Moya-Diaz *et al.* 2016), a subpopulation of IRP that recovers very rapidly. More importantly, the results indicate that the rapid component of IRP replenishment is accelerated by the low cytosolic $[Ca^{2+}]$ promoted at high BAPTA (Figures 4 and 5). Moreover, the decrease in cytosolic Ca^{2+} also potentiates the speed and magnitude of fast endocytosis that precedes the replenishment (Figure 3). Additionally, our results show that application of intracellular 500 nM Ca^{2+} abolished fast endocytosis and reduced the replenishment of IRP to only one relatively slow component (Figure 2). In light of our present knowledge, the fact that fast endocytosis is facilitated at low cytosolic $[Ca^{2+}]$ can be interpreted in two different ways. One possibility is that Ca^{2+} directly inhibits endocytosis, as previously reported for goldfish retinal bipolar neurons, calyx of Held and bovine chromaffin cells (von Gersdorff & Matthews 1994; Wu & Wu 2014; Chan *et al.* 2003). Moreover, our results indicate that the facilitation of endocytosis by BAPTA is due to the decrease in basal $[Ca^{2+}]i$, and is not related to the increment in I_{Ca2+} (Figure 3 and Supplementary Figure 2). This is in agreement with the findings of Wu and Wu (2014), who concluded that prolonged, small, and global increases of cytosolic $[Ca^{2+}]$ inhibit endocytosis. Another possibility is that low cytosolic $[Ca^{2+}]$ favors a "kiss-and-run" like exocytotic mechanism followed by fast endocytosis, while higher $[Ca^{2+}]$ promotes full fusion (Fulop *et al.* 2005; Elhamdani *et al.* 2006; Chan *et al.* 2003; Chan & Smith 2001). Since "kiss-and-run" is associated with a short and fast recycling of vesicles (Alabi & Tsien 2013), this second hypothesis can also explain why IRP is replenished rapidly. The cellular mechanisms of these processes are unknown, but they might be related with the effect of Ca^{2+} on cortical F-actin cytoskeleton (Supplementary Figure 3B). The increase in BAPTA reduces cytosolic basal $[Ca^{2+}]$, and this in turn increases F-actin density. It was demonstrated by several authors that the dynamics of the cell actin network is regulated by cytosolic Ca^{2+} (Olivares *et al.* 2014; Rodriguez Del Castillo *et al.* 1990; Doreian *et al.* 2008). In addition, cortical F-actin is a

recognized assistant molecule for membrane retrieval (Gormal *et al.* 2015; Watanabe *et al.* 2013; Boulant *et al.* 2011), and also favors the "kiss-and-run" mode of fusion (Doreian *et al.* 2008).

Rapid Replenishment and Fast Endocytosis Depend on Cortical F-actin

Several actin depolymerizing and severing enzymes, as for example cofilin, gelsolin, scinderin and villin, are modulated by Ca^{2+} (Lueck *et al.* 2000; Rodriguez Del Castillo *et al.* 1990; Kumar *et al.* 2004), (Wang *et al.* 2005). Our results indicate that increase in cytosolic Ca^{2+}, in the range 0.01-1 µM, provokes disruption of cortical F-actin (Supplementary Figure 3B), reduction and deceleration of fast endocytosis and also deceleration of rapid replenishment (Figures 2-5). At 4 mM BAPTA (approximately 0.02 µM Ca^{2+}) we obtained both the fastest and largest endocytosis, and the fastest replenishment. Under this condition we found that disruption of cortical F-actin with Cyto D treatment slowed down endocytosis and replenishment, reverting in part the effect of high BAPTA (Figure 7). Therefore, it seems that the polymerized cortical F-actin is important for the development of fast endocytosis and rapid replenishment. This conclusion is also supported by the effect of Cyto D on fast endocytosis and rapid replenishment after ETAP exocytosis (Figure 8).

Several endocytic mechanisms depend on cortical F-actin cytoskeleton. Particularly bulk endocytosis, classical clathrin-mediated endocytosis, and ultrafast endocytosis need or at least are partially supported by F-actin (Gormal *et al.* 2015; Watanabe *et al.* 2013; Boulant *et al.* 2011). Bulk endocytosis is a massive membrane internalization induced by strong stimulation (Perez Bay *et al.* 2007; Perez Bay *et al.* 2012; Gormal *et al.* 2015), which is totally different to our experimental conditions. Clathrin-mediated endocytosis is triggered by more moderate stimuli than bulk endocytosis, although stronger than those applied in this work, and presents slower kinetics (Chan & Smith 2003; Artalejo *et al.* 2002; Hosoi *et al.* 2009). On the other hand, ultrafast endocytosis is completed in few hundreds of milliseconds in hyppocampal synapses and is dependent on dynamin and F-actin, which is compatible with our results (Watanabe *et al.* 2013). However, ultrafast endocytosis has not been demonstrated in chromaffin cells and it is activated at 37 ºC (Watanabe *et al.* 2014), but not at room temperature (the condition of the present work). An alternative possibility is that the disruption of F-actin by Cyto D inhibits the "kiss-and-run" mode of vesicle fusion and promotes full collapse (Doreian *et al.* 2008). This is a plausible hypothesis that can describe our data, since the retrieval of vesicles after "kiss-and-run" is kinetically manifested as fast endocytosis (Elhamdani *et al.* 2006; Wu *et al.* 2014).

Classically, three vesicle recycling pathways were proposed in synaptic terminals. Two fast pathways in which vesicles either remain at the active zone for refilling ("kiss-and-stay") or are recycled locally ("kiss-and-run"), and a slower pathway that involves clathrin-mediated endocytosis (Sudhof 2004). Application of short depolarizations at low frequencies induces a kiss–and-run mode of fusion (Fulop *et al.* 2005; Ceccarelli *et al.* 1973; Cardenas & Marengo 2016) and fast endocytosis (Chan & Smith 2003; Chan & Smith 2001; Sun *et al.* 2002). A simple way to interpret our results is to consider that organized cortical F-actin promotes "kiss-and-run", and consequently fast endocytosis and a rapid local recycling of vesicles (Doreian *et al.* 2008; Moya-Diaz *et al.* 2016). Therefore, we can expect that disruption of F-actin with Cyto D will affect the whole process. Alternatively, Hosoi and collaborators (2009), working with the calyx of Held, proposed that after exocytosis a fast endocytotic mechanism may facilitate rapid vesicle replenishment by clearance of exocytotic materials from active zones, restoring the structure of the release sites. This concept was also proposed by Wu and collaborators to explain deceleration of endocytosis and RRP replenishment by the knocking out of β-actin in the calyx of Held (Wu *et al.* 2016). In accordance with this hypothesis, if endocytosis is impaired by F-actin disruption (or by inhibition of dynamin) vesicle replenishment will be affected as well. Finally, we have to consider the possible contribution to vesicle replenishment of cortical actomyosin relaxation promoted by cell stimulation, as was proposed by Papadopulos and coworkers (2015). Relaxation of cortical actomyosin translocates attached secretory vesicles towards docking sites in the plasma membrane. Treatment with Cyto D releases part of the tension existing at rest, partially inhibiting vesicle translocation induced by the stimulus.

At rest, chromaffin cells fire action potentials at low frequencies, Ca^{2+} does not accumulate between stimuli and exocytosis would be limited to vesicles closely coupled to VDCC (Alvarez & Marengo 2011; Voets *et al.* 1999). It is likely that the physiological importance of IRP resides in its highly efficient stimulus-exocytosis coupling, which allows secretion during action potentials at low rate (Oré & Artalejo 2005; Cardenas & Marengo 2016). IRP is a small pool of vesicles, and is almost 50% depleted by a single action potential (Moya-Diaz *et al.* 2016). Sustained participation of IRP in chromaffin cell exocytosis during repetitive stimulation depends on the refilling rate of this pool. Therefore, IRP would need a rapid replenishment mechanism compatible with physiological basal action potential frequencies. The rapid component of IRP replenishment described in this work might be part of the solution.

Acknowledgments

Conflict of interest

The authors have no conflicts of interest to declare.

Figure Legends

Figure 1. The replenishment of IRP involves two kinetic components. A (i), Scheme of the stimulation protocol. In order to determine the kinetics of IRP replenishment, a pair of 50 ms depolarizations ($SQR50_1$ and $SQR50_2$) (from -80 to +10 mV) with a variable time interval between them was applied. (ii) $I_{Ca^{2+}}$ and (iii) Cm recordings obtained during a typical experiment when a 5 s interval between stimuli was applied. The white line in (iii) represents a single exponential fit $\left(\Delta Cm = Yo + A . e^{-\frac{t}{\tau_{endo}}}\right)$ applied to the decay in Cm, where Yo=9.8±0.1 fF, A=14±0.2 fF, and τ_{endo}=1.17±0.03 s, R>0.837. B, The relative replenishment of IRP after depletion (expressed as averages of $\Delta Cm_2/\Delta Cm_1$ for every time interval) was plotted against the time interval between 50 ms depolarizations and fitted to a biexponential growing function of the form $\frac{\Delta C_{m2}}{\Delta C_{m1}} = Y_0 + A_I.\left(1 - e^{-\frac{t}{\tau_{R1}}}\right) + A_{II}.\left(1 - e^{-\frac{t}{\tau_{R2}}}\right)$, where Y_0= 0.30±0.02, A_I=0.32±0.04, τ_{R1}=1.07±0.27 s, A_{II}=0.37±0.04, and τ_{R2}=10.42±2.55 s, R>0.998. The points represented in the plot are averages of all the measurements obtained in individual cells (one measurement per cell), and the number of measurements included in each point is represented in the Supplementary Table 2. The fitting was performed on average values.

Figure 2. Effects of high cytosolic [Ca^{2+}] on fast endocytosis and IRP replenishment: A, Typical Cm recording obtained from a cell dialyzed with 500 nM Ca^{2+} in the internal solution. In this example, the interval between stimuli (50 ms depolarizations from -80 to +10 mV) was 5 s. B, The relative replenishment after depletion (expressed as averages of $\Delta Cm_2/\Delta Cm_1$ for every time interval) was plotted against the time interval between depolarizations and fitted to a single exponential growing function of the form $\frac{\Delta C_{m2}}{\Delta C_{m1}} = Y_0 + A.\left(1 - e^{-\frac{t}{\tau}}\right)$, where Y_0=0.43±0.02, A=0.60±0.04 and τ_R=5.22±0.89 s, R>0.986. The number of measurements (one measurement per cell) included in each point on the plot is represented in the Supplementary Table 2. The fitting was performed on average values.

Figure 3. Effect of the increase in Ca^{2+} buffer capacity on fast endocytosis: A, Typical Cm recordings obtained from two cells dialyzed with 0.5 and 4 mM cytosolic BAPTA in the internal

solution, respectively. The white lines represent the single exponential fits ($\Delta Cm = Yo + A \cdot e^{-\frac{t}{\tau}}$) applied to the decay in Cm in both conditions (R>0.843 and R>0.871, respectively). B-F, The plots represent average values, standard errors and individual measurements (1 measurement/cell) of I_{Ca2+}, exocytosis (ΔCm_{exo}), endocytosis (ΔCm_{endo}), ratio between endocytosis and exocytosis (endo/exo), and time constant of endocytosis (τ_{endo}) obtained at 0.5, 1, 2 and 4 mM BAPTA, respectively. The data were analyzed by single way ANOVA (B, E, F), or Kruskal-Wallis one way analysis of variance on ranks (C, D). The comparisons were always done against 0.5 BAPTA. * p<0.05. The number of cells averaged in each condition is represented between parentheses.

Figure 4. Effect of Ca²⁺ buffer capacity on IRP replenishment: A-D, The relative replenishment after depletion (expressed as averages of $\Delta Cm_2/\Delta Cm_1$ for every time interval) was plotted against the time interval between depolarizations and fitted to a single exponential growing function of the form $\frac{\Delta C_{m2}}{\Delta C_{m1}} = Y_0 + A \cdot \left(1 - e^{-\frac{t}{\tau}}\right)$, for 0.5 (R>0.976), 1 (R>0.941), 2 (R>0.976) and 4 mM BAPTA (R>0.946), in that order. The number of measurements (one measurement per cell) included in each point on the plots is represented in the Supplementary Table 2. The fittings were performed on average values.

Figure 5. Effect of Ca²⁺ buffer capacity on IRP replenishment: A (i) and (ii), The relative replenishment after depletion obtained in two cells dialyzed with 0.5 and 4 mM BAPTA respectively is plotted against the time interval between depolarizations, and fitted to a single exponential growing function of the form $\frac{\Delta C_{m2}}{\Delta C_{m1}} = Y_0 + A \cdot \left(1 - e^{-\frac{t}{\tau}}\right)$. The correlation coefficient R was bigger than 0.943 and 0.990, respectively. B, The plot represents average values, standard errors and individual measurements (1 measurement/cell) of the time constant of replenishment (τ_R) obtained at 0.5, 1, 2 and 4 mM BAPTA, respectively. The data was analyzed by single way ANOVA followed by Bonferroni. The comparisons were done against 0.5 BAPTA. * p<0.05. The number of cells averaged in each condition is represented between parentheses.

Figure 6. The inhibition of dynamin decelerates both fast endocytosis and rapid replenishment: A, Typical Cm recordings obtained from a control cell dialyzed with 4 mM

cytosolic BAPTA (i) and another cell dialyzed with 4 mM cytosolic BAPTA plus a monoclonal antibody against dynamin (antiDyn, ii) (see methods). The white lines represent single exponential fits ($\Delta Cm = Yo + A.e^{-\frac{t}{\tau}}$) applied to the decay in Cm for control (R>0.863) and antiDyn (R>0.931), respectively. All the cells were dialyzed with the internal solution during 5 min before starting with the measurements. B, The relative replenishment after depletion (expressed as averages of $\Delta Cm_2/\Delta Cm_1$ for every time interval) is plotted against the time interval between depolarizations and fitted to a single exponential growing function of the form $\frac{\Delta C_{m2}}{\Delta C_{m1}} = Y_0 + A.\left(1 - e^{-\frac{t}{\tau}}\right)$ for the control condition (R>0.992) (i) and for antiDyn (R>0.893) (ii), respectively. The number of measurements (one measurement per cell) included in each point on the plots is represented in the Supplementary Table 2. The fittings were performed on average values. C, The relative replenishment obtained in two cells, one in the control condition (R>0.980) (i) and the other one dialyzed with antiDyn (R>0.945) (ii), are plotted against the time interval between depolarizations and fitted to a single exponential growing function of the same form as represented above.

Figure 7: Effects of F-actin disruption on fast endocytosis and IRP replenishment: A, Confocal images of rhodamine-phalloidin associated fluorescence distribution in cells under control conditions or after pretreatment with 2 μM cytochalasin D (Cyto D) during 10 min at 37°C. Three representative cells for each condition are shown. Nuclei, stained with DAPI, are shown in blue. B, Typical Cm recordings obtained from a control cell dialyzed with 4 mM cytosolic BAPTA (i), and another cell dialyzed with 4 mM cytosolic BAPTA after a pretreatment with Cyto D (ii). The white lines represent single exponential fits ($\Delta Cm = Yo + A.e^{-\frac{t}{\tau}}$) applied to the decay in Cm for control (R>0.938) and Cyto D (R>0.863), respectively. C, The relative replenishment after depletion (expressed as averages of $\Delta Cm_2/\Delta Cm_1$ for every time interval) is plotted against the time interval between depolarizations and fitted to a single exponential growing function of the form $\frac{\Delta C_{m2}}{\Delta C_{m1}} = Y_0 + A.\left(1 - e^{-\frac{t}{\tau}}\right)$ for the control condition (R>0.988) (i) and for Cyto D (R>0.970) (ii), respectively. The number of measurements (one measurement per cell) included in each point on the plots is represented in the Supplementary Table 2. The fittings were performed on average values.

Figure 8: Effects of F-actin disruption on fast endocytosis and ETAP replenishment: A, Scheme of APls depolarization (i), I_{Ca2+} (ii) and Cm recordings (iii) obtained during typical experiments performed in control conditions (left) and after a pretreatment with Cyto D (right), respectively. The white lines represent single exponential fits ($\Delta Cm = Yo + A \cdot e^{-\frac{t}{\tau}}$) applied to the decay in Cm for control (R>0.763) and Cyto D (R>0.804), respectively. B (i) and (ii), The relative replenishment of ETAP after depletion (expressed as averages of $\Delta Cm_2/\Delta Cm_1$ for every time interval) is plotted against the time interval between depolarizations and fitted to a single exponential growing function of the form $\frac{\Delta C_{m2}}{\Delta C_{m1}} = Y_0 + A \cdot \left(1 - e^{-\frac{t}{\tau}}\right)$ for the control condition (R>0.997) and for Cyto D (R>0.990) (ii), respectively. The number of measurements (one measurement per cell) included in each point on the plots is represented in the Supplementary Table 2. The fittings were performed on average values.

Table 1

	CONTROL	500 nM Ca^{2+}
I$_{Ca2+}$ (pA)	163±19 (28)	101±14 (24) *MW
ΔC$_m$ **exo** (fF)	21±2 (28)	22±3 (24)
ΔC$_m$ **endo** (fF)	9±2 (21)	-0.27±2.16 (17) *ST
endo/exo	0.45±0.06 (21)	-0.12±0.17 (17) *MW

* $p < 0.05$

Average values of Ca^{2+} current (I$_{Ca2+}$), exocytosis (ΔC$_m$ exo), endocytosis (ΔC$_m$ endo) and endo/exo ratio for control conditions (5 mM Ca^{2+} in the external solution and 0.5 mM EGTA in the internal solution) and for cells dialyzed with 500 nM free Ca^{2+} in the internal solution. The number of cells measured in each condition is between parentheses. The data were analyzed by Student's "t" (ST) or Mann-Whitney (MW) test for comparisons between two groups of independent data samples.

Table 2

	CONTROL	4 mM BAPTA+antiDyn
I_{Ca} (pA)	252±37 (9)	247±40 (10)
ΔC_m **exo** (fF)	13±2 (9)	9±1 (10) *ST
ΔC_m **endo** (fF)	13±2 (9)	9±1 (10)
endo/exo	1.00±0.05 (9)	0.98±0.11 (10)
τ_{endo} (s)	0.79±0.12 (9)	1.39±0.17 (10) *MW
τ_R (s)	0.69±0.11 (9)	1.5±0.19 (10) *ST

* p < 0.05

Average values of Ca^{2+} current (I_{Ca2+}), exocytosis (ΔC_m exo), endocytosis (ΔC_m endo), endo/exo ratio, time constant of endocytosis (τ_{endo}) and the time constant of replenishment (τ_R) for cells dialyzed with a monoclonal antibody against dynamin in the internal solution (4 mM BAPTA+antiDyn, right), and their respective control conditions (4 mM BAPTA in the internal solution, left). The number of cells measured in each condition is between parentheses. The data were analyzed by Student's "t" (ST) or Mann-Whitney (MW) test for comparisons between two groups of independent data samples.

Table 3

	SQR50/BAPTA 4 mM		APls/EGTA 0.5 mM	
	CONTROL	**Cyto D**	**CONTROL**	**Cyto D**
I_{Ca} (pA)	221±25 (10)	227±29 (12)	336± 32 (10)	363± 39 (12)
ΔC_m **exo** (fF)	14±2 (10)	8±1 (12) *MW	8±1 (10)	7±1 (12)
ΔC_m **endo** (fF)	14±3 (10)	9±1 (12) *MW	7±1 (10)	6±1 (12)
endo/exo	0.97±0.07 (10)	1.11±0.04 (12)	0.89±0.05 (10)	0.93±0.05 (12)
$\tau_{endo\,(s)}$	0.73±0.09 (9)	1.09±0.11 (12)*ST	0.82±0.08 (10)	1.24±0.08 (12)*ST
τ_R (s)	0.63±0.06 (10)	1.17±0.15 (9)*ST	0.85±0.10 (10)	1.64±0.29 (9)*MW

* $p < 0.05$

Average values of Ca^{2+} current (I_{Ca2+}), exocytosis (ΔC_m exo), endocytosis (ΔC_m endo), endo/exo ratio, time constant of endocytosis (τ_{endo}) and time constant of replenishment (τ_R) for cells stimulated with a square 50 ms depolarization (SQR50, two columns on the left), or an action potential like stimulus (APls, two columns on the right), in their respective control conditions and after a pretreatment with cytochalasin D (Cyto D). The internal solutions of SQRT experiments were buffered with 4 mM BAPTA, and the internal solutions of APls experiments were buffered with 0.5 EGTA. The number of cells measured in each condition is between parentheses. The data were analyzed by Student's "t" (ST) or Mann-Whitney (MW) test for comparisons between two groups of independent data samples. The comparisons were made between each Cyto D group and their respective control group.

References

Alabi, A. A. and Tsien, R. W. (2013) Perspectives on kiss-and-run: role in exocytosis, endocytosis, and neurotransmission. *Ann. Rev. Physiol.* **75,** 393-422.

Alvarez, Y. D., Belingheri, V. A., Perez Bay, A. E., Javis, S. E., Tedford, H. W., Zamponi, G. W. and Marengo, F. D. (2013) The Immediately Releasable Pool of Mouse Chromaffin Cell Vesicles Is Coupled to P/Q-Type Calcium Channels via the Synaptic Protein Interaction Site. *PLoS.One.* **8** e54846.

Alvarez, Y. D., Ibanez, L. I., Uchitel, O. D. and Marengo, F. D. (2008) P/Q Ca2+ channels are functionally coupled to exocytosis of the immediately releasable pool in mouse chromaffin cells. *Cell Calcium* **43,** 155-164.

Alvarez, Y. D. and Marengo, F. D. (2011) The immediately releasable vesicle pool: highly coupled secretion in chromaffin and other neuroendocrine cells. *J. Neurochem.* **116,** 155-163.

Artalejo, C. R., Elhamdani, A. and Palfrey, H. C. (2002) Sustained stimulation shifts the mechanism of endocytosis from dynamin-1-dependent rapid endocytosis to clathrin- and dynamin-2-mediated slow endocytosis in chromaffin cells. *Proc. Natl. Acad. Sci. U.S.A* **99,** 6358-6363.

Becherer, U., Moser, T., Stuhmer, W. and Oheim, M. (2003) Calcium regulates exocytosis at the level of single vesicles. *Nat. Neurosci.* **6,** 846-853.

Boulant, S., Kural, C., Zeeh, J. C., Ubelmann, F. and Kirchhausen, T. (2011) Actin dynamics counteract membrane tension during clathrin-mediated endocytosis. *Nat. Cell Biol.* **13,** 1124-1131.

Cardenas, A. M. and Marengo, F. (2016) How the stimulus defines the dynamics of vesicle pool recruitment, fusion mode and vesicle recycling in neuroendocrine cells. *J. Neurochem.* **137**, 867—879.

Ceccarelli, B., Hurlbut, W. P. and Mauro, A. (1973) Turnover of transmitter and synaptic vesicles at the frog neuromuscular junction. *J. Cell. Biol.* **57,** 499-524.

Chan, S. A., Chow, R. and Smith, C. (2003) Calcium dependence of action potential-induced endocytosis in chromaffin cells. *Pflugers Arch.* **445,** 540-546.

Chan, S. A., Polo-Parada, L., Landmesser, L. T. and Smith, C. (2005) Adrenal chromaffin cells exhibit impaired granule trafficking in NCAM knockout mice. *J. Neurophysiol.* **94,** 1037-1047.

Chan, S. A. and Smith, C. (2001) Physiological stimuli evoke two forms of endocytosis in bovine chromaffin cells. *J. Physiol.* **537,** 871-885.

Chan, S. A. and Smith, C. (2003) Low frequency stimulation of mouse adrenal slices reveals a clathrin-independent, protein kinase C-mediated endocytic mechanism. *J. Physiol.* **553,** 707-717.

de Diego, A. M., Gandia, L. and Garcia, A. G. (2008) A physiological view of the central and peripheral mechanisms that regulate the release of catecholamines at the adrenal medulla. *Acta Physiol. (Oxf)* **192,** 287-301.

Doreian, B. W., Fulop, T. G. and Smith, C. B. (2008) Myosin II activation and actin reorganization regulate the mode of quantal exocytosis in mouse adrenal chromaffin cells. *J. Neurosci.* **28,** 4470-4478.

Elhamdani, A., Azizi, F. and Artalejo, C. R. (2006) Double patch clamp reveals that transient fusion (kiss-and-run) is a major mechanism of secretion in calf adrenal chromaffin cells: high calcium shifts the mechanism from kiss-and-run to complete fusion. *J. Neurosci.* **26,** 3030-3036.

Fulop, T., Radabaugh, S. and Smith, C. (2005) Activity-dependent differential transmitter release in mouse adrenal chromaffin cells. *J. Neurosci.* **25,** 7324-7332.

Gillis, K. D. (1995) Techniques for membrane capacitance measurements. *Single-channel Recording , Ed 2 (Sakmann B., Neher E., eds), pp. 155 - 198. Plenum, New York.*

Gomis, A., Burrone, J. and Lagnado, L. (1999) Two actions of calcium regulate the supply of releasable vesicles at the ribbon synapse of retinal bipolar cells. *J Neurosci.* **19,** 6309-6317.

Gonzalez-Jamett, A. M., Baez-Matus, X., Hevia, M. A., Guerra, M. J., Olivares, M. J., Martinez, A. D., Neely, A. and Cardenas, A. M. (2010) The association of dynamin with synaptophysin regulates quantal size and duration of exocytotic events in chromaffin cells. *J Neurosci.* **30,** 10683-10691.

Gormal, R. S., Nguyen, T. H., Martin, S., Papadopulos, A. and Meunier, F. A. (2015) An acto-myosin II constricting ring initiates the fission of activity-dependent bulk endosomes in neurosecretory cells. *J Neurosci.* **35,** 1380-1389.

Grynkiewicz, G., Poenie, M. and Tsien, R. Y. (1985) A new generation of Ca2+ indicators with greatly improved fluorescence properties. *J. Biol. Chem.* **260,** 3440-3450.

Heinemann, C., von Ruden, L., Chow, R. H. and Neher, E. (1993) A two-step model of secretion control in neuroendocrine cells. *Pflugers Archiv* **424,** 105-112.

Holman, M. E., Coleman, H. A., Tonta, M. A. and Parkington, H. C. (1994) Synaptic transmission from splanchnic nerves to the adrenal medulla of guinea-pigs. *J. Physiol.* **478 (Pt 1),** 115-124.

Horrigan, F. T. and Bookman, R. J. (1994) Releasable pools and the kinetics of exocytosis in adrenal chromaffin cells. *Neuron* **13,** 1119-1129.

Hosoi, N., Holt, M. and Sakaba, T. (2009) Calcium dependence of exo- and endocytotic coupling at a glutamatergic synapse. *Neuron* **63,** 216-229.

Kumar, N., Tomar, A., Parrill, A. L. and Khurana, S. (2004) Functional dissection and molecular characterization of calcium-sensitive actin-capping and actin-depolymerizing sites in villin. *J. Biol. Chem.* **279,** 45036-45046.

Li, P., Bademosi, A. T., Luo, J. and Meunier, F. A. (2018) Actin Remodeling in Regulated Exocytosis: Toward a Mesoscopic View. *Trends Cell Biol.* **28,** 685-697.

Lueck, A., Yin, H. L., Kwiatkowski, D. J. and Allen, P. G. (2000) Calcium regulation of gelsolin and adseverin: a natural test of the helix latch hypothesis. *Biochemistry* **39,** 5274-5279.

Marcantoni, A., Vandael, D. H., Mahapatra, S., Carabelli, V., Sinnegger-Brauns, M. J., Striessnig, J. and Carbone, E. (2010) Loss of Cav1.3 channels reveals the critical role of L-type and BK channel coupling in pacemaking mouse adrenal chromaffin cells. *J Neurosci.* **30,** 491-504.

Marengo, F. D. (2005) Calcium gradients and exocytosis in bovine adrenal chromaffin cells. *Cell Calcium* **38,** 87-99.

Moser, T. and Neher, E. (1997) Rapid exocytosis in single chromaffin cells recorded from mouse adrenal slices. *J Neurosci.* **17,** 2314-2323.

Moya-Diaz, J., Alvarez, Y. D., Montenegro, M., Bayones, L., Belingheri, A. V., Gonzalez-Jamett, A. M., Cardenas, A. M. and Marengo, F. D. (2016) Sustained Exocytosis after Action Potential-Like Stimulation at Low Frequencies in Mouse Chromaffin Cells Depends on a Dynamin-Dependent Fast Endocytotic Process. *Front. Cell. Neurosci.* **10,** 184.

Moya-Diaz, J., Bayones, L., Montenegro, M., Cardenas, A. M., Koch, H., Doi, A. and Marengo, F. D. (2020) Ca(2+) -independent and voltage-dependent exocytosis in mouse chromaffin cells. *Acta Physiol. (Oxf)* **228,** e13417.

Olivares, M. J., Gonzalez-Jamett, A. M., Guerra, M. J., Baez-Matus, X., Haro-Acuna, V., Martinez-Quiles, N. and Cardenas, A. M. (2014) Src kinases regulate de novo actin polymerization during exocytosis in neuroendocrine chromaffin cells. *PloS one* **9,** e99001.

Oré, L. O. and Artalejo, A. R. (2005) Intracellular Ca2+ microdomain-triggered exocytosis in neuroendocrine cells. *Trends Neurosci.* **27** 113-115.

Papadopulos, A., Gomez, G. A., Martin, S., Jackson, J., Gormal, R. S., Keating, D. J., Yap, A. S. and Meunier, F. A. (2015) Activity-driven relaxation of the cortical actomyosin II network synchronizes Munc18-1-dependent neurosecretory vesicle docking. *Nat. Commun.* **6,** 6297.

Perez Bay, A. E., Belingheri, A. V., Alvarez, Y. D. and Marengo, F. D. (2012) Membrane cycling after the excess retrieval mode of rapid endocytosis in mouse chromaffin cells. *Acta Physiol (Oxf)* **204,** 403-418.

Perez Bay, A. E., Ibanez, L. I. and Marengo, F. D. (2007) Rapid recovery of releasable vesicles and formation of nonreleasable endosomes follow intense exocytosis in chromaffin cells. *Am J Physiol Cell Physiol* **293,** C1509-1522.

Rodriguez Del Castillo, A., Lemaire, S., Tchakarov, L., Jeyapragasan, M., Doucet, J. P., Vitale, M. L. and Trifaro, J. M. (1990) Chromaffin cell scinderin, a novel calcium-dependent actin filament-severing protein. *The EMBO Journal* **9,** 43-52.

Rose, S. D., Lejen, T., Zhang, L. and Trifaro, J. M. (2001) Chromaffin cell F-actin disassembly and potentiation of catecholamine release in response to protein kinase C activation by phorbol esters is mediated through myristoylated alanine-rich C kinase substrate phosphorylation. *J. Biol. Chem.* **276,** 36757-36763.

Shin, W., Ge, L., Arpino, G. et al. (2018) Visualization of Membrane Pore in Live Cells Reveals a Dynamic-Pore Theory Governing Fusion and Endocytosis. *Cell* **173,** 934-945 e912.

Sokal, R. and Rohlf, F. (2009) Statistical Tables. In: *Introduction to Biostatistics,* pp. 321-321. Dover Publications, Mineola, New York.

Sorensen, J. B. (2004) Formation, stabilisation and fusion of the readily releasable pool of secretory vesicles. *Pflugers Archiv* **448,** 347-362.

Sudhof, T. C. (2004) The synaptic vesicle cycle. *Ann. Rev. Neurosci.* **27,** 509-547.

Sun, J. Y., Wu, X. S. and Wu, L. G. (2002) Single and multiple vesicle fusion induce different rates of endocytosis at a central synapse. *Nature* **417,** 555-559.

Trifaro, J. M., Gasman, S. and Gutierrez, L. M. (2008) Cytoskeletal control of vesicle transport and exocytosis in chromaffin cells. *Acta Physiol (Oxf)* **192,** 165-172.

Voets, T., Neher, E. and Moser, T. (1999) Mechanisms underlying phasic and sustained secretion in chromaffin cells from mouse adrenal slices. *Neuron* **23,** 607-615.

von Gersdorff, H. and Matthews, G. (1994) Inhibition of endocytosis by elevated internal calcium in a synaptic terminal. *Nature* **370,** 652-655.

Wallace, D. J., Chen, C. and Marley, P. D. (2002) Histamine promotes excitability in bovine adrenal chromaffin cells by inhibiting an M-current. *J. Physiol.* **540,** 921-939.

Wang, Y., Shibasaki, F. and Mizuno, K. (2005) Calcium signal-induced cofilin dephosphorylation is mediated by Slingshot via calcineurin. *J. Biol. Chem.* **280,** 12683-12689.

Watanabe, S., Rost, B. R., Camacho-Perez, M., Davis, M. W., Sohl-Kielczynski, B., Rosenmund, C. and Jorgensen, E. M. (2013) Ultrafast endocytosis at mouse hippocampal synapses. *Nature* **504,** 242-247.
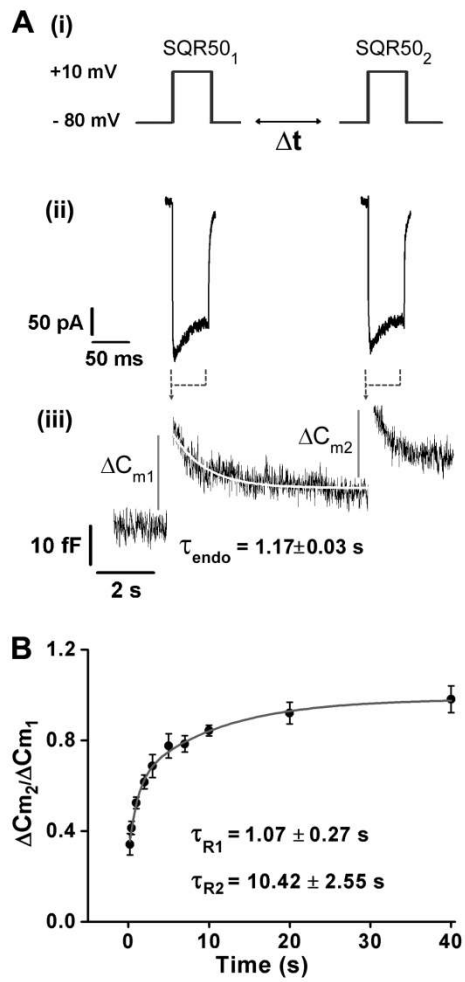
Watanabe, S., Trimbuch, T., Camacho-Perez, M. et al. (2014) Clathrin regenerates synaptic vesicles from endosomes. *Nature* **515,** 228-233.

Wu, L. G., Hamid, E., Shin, W. and Chiang, H. C. (2014) Exocytosis and endocytosis: modes, functions, and coupling mechanisms. *Annu. Rev. Physiol.* **76,** 301-331.

Wu, X. S., Lee, S. H., Sheng, J. et al. (2016) Actin Is Crucial for All Kinetically Distinguishable Forms of Endocytosis at Synapses. *Neuron* **92,** 1020-1035.
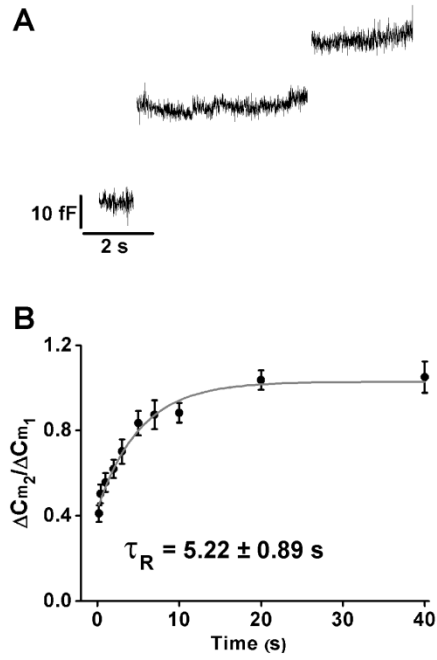
Wu, X. S. and Wu, L. G. (2014) The yin and yang of calcium effects on synaptic vesicle endocytosis. *J Neurosci.* **34,** 2652-2659.
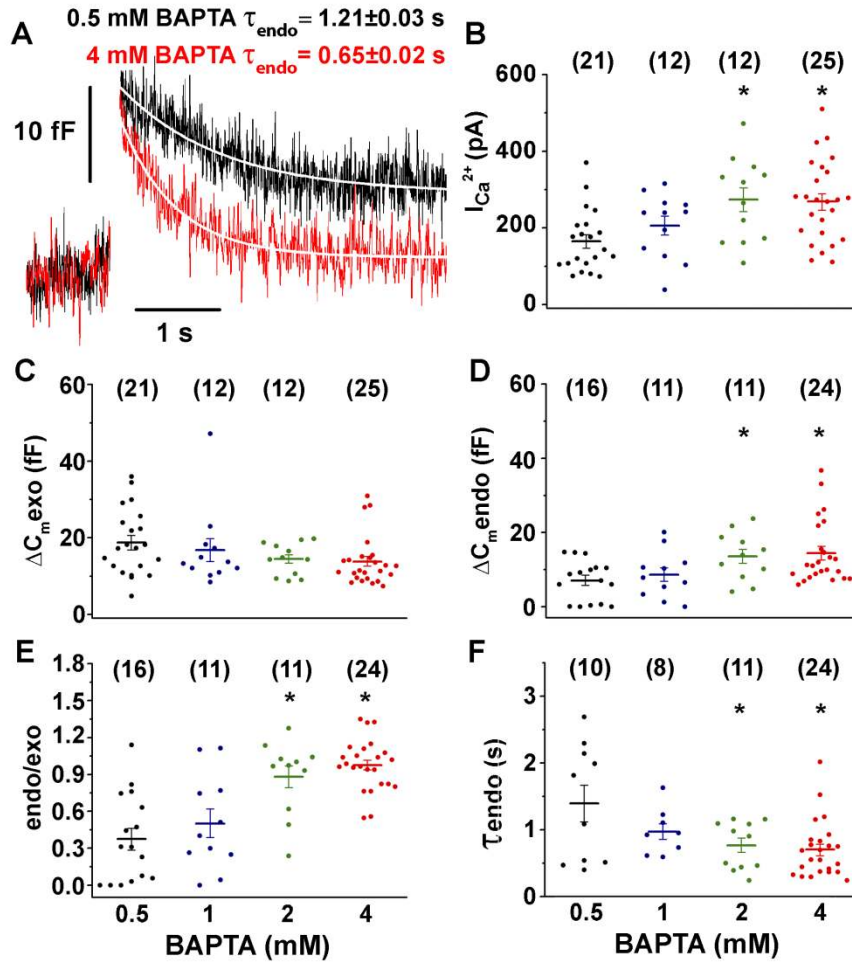
Figure 1

A (i)

SQR50$_1$ SQR50$_2$

+10 mV

- 80 mV

Δt

(ii)

50 pA

50 ms

(iii)

ΔC_{m2}

ΔC_{m1}

10 fF

τ_{endo} = 1.17±0.03 s

2 s

B

τ_{R1} = 1.07 ± 0.27 s

τ_{R2} = 10.42 ± 2.55 s

Time (s)

jnc_15276_f1.tif

Figure 2

A

10 fF

2 s

B

$\Delta C_{m_2}/\Delta C_{m_1}$

Time (s)

$\tau_R = 5.22 \pm 0.89$ s

jnc_15276_f2.tif

Figure 3

jnc_15276_f3.tif

Figure 4

jnc_15276_f4.tif

Figure 5

A (i)

0.5 mM BAPTA $\quad \tau_R = 1.75 \pm 0.63$ s

(ii)

4 mM BAPTA $\quad \tau_R = 0.53 \pm 0.11$ s

B

jnc_15276_f5.tif

Figure 6

4 mM BAPTA

4 mM BAPTA + antiDyn

A

(i) $\tau_{endo} = 0.66 \pm 0.01$ s

(ii) $\tau_{endo} = 1.22 \pm 0.02$ s

5 fF

1 s

B

$\Delta Cm_1 / \Delta Cm_2$

(i)

$\tau_R = 0.76 \pm 0.11$ s

(ii)

$\tau_R = 1.31 \pm 0.25$ s

C

$\Delta Cm_1 / \Delta Cm_2$

(i)

$\tau_R = 0.56 \pm 0.14$ s

Time (s)

(ii)

$\tau_R = 1.47 \pm 0.54$ s

Time (s)

jnc_15276_f6.tif

Figure 7

A

CONTROL   Cyto D

10 μm

B (i) 4 mM BAPTA   (ii) 4 mM BAPTA + Cyto D

$\tau_{endo}=0.86\pm0.01$ s $\tau_{endo}=1.25\pm0.03$ s

10 fF

1 s

C (i)   (ii)

$\tau_R = 0.71 \pm 0.12$ s $\tau_R = 1.33 \pm 0.35$ s

$\Delta Cm_1/\Delta Cm_2$

Time (s)
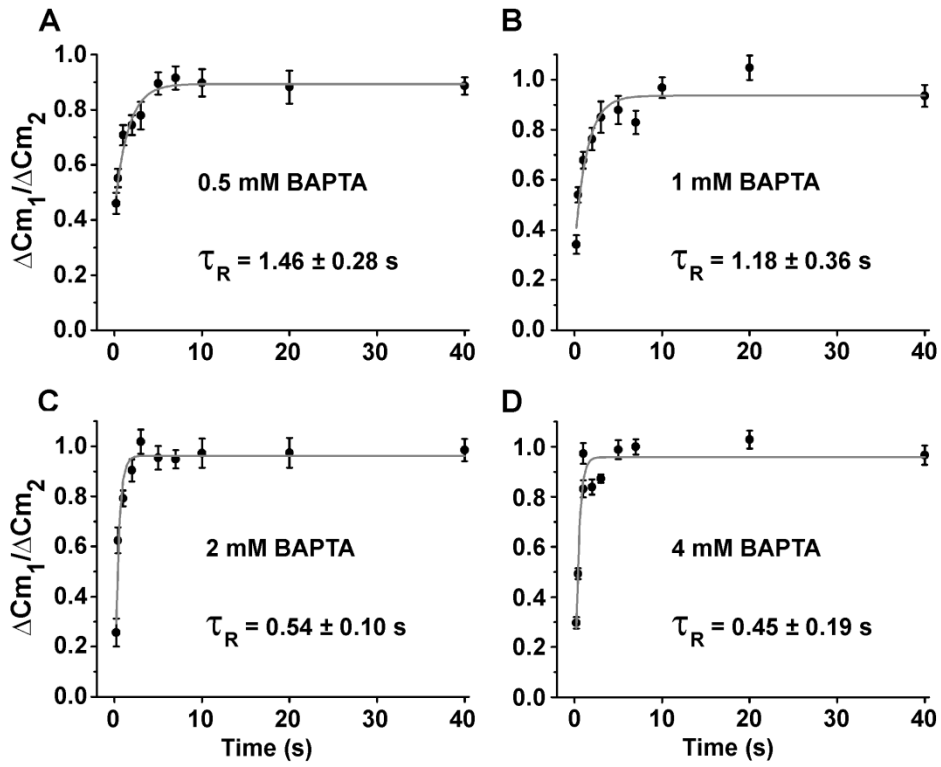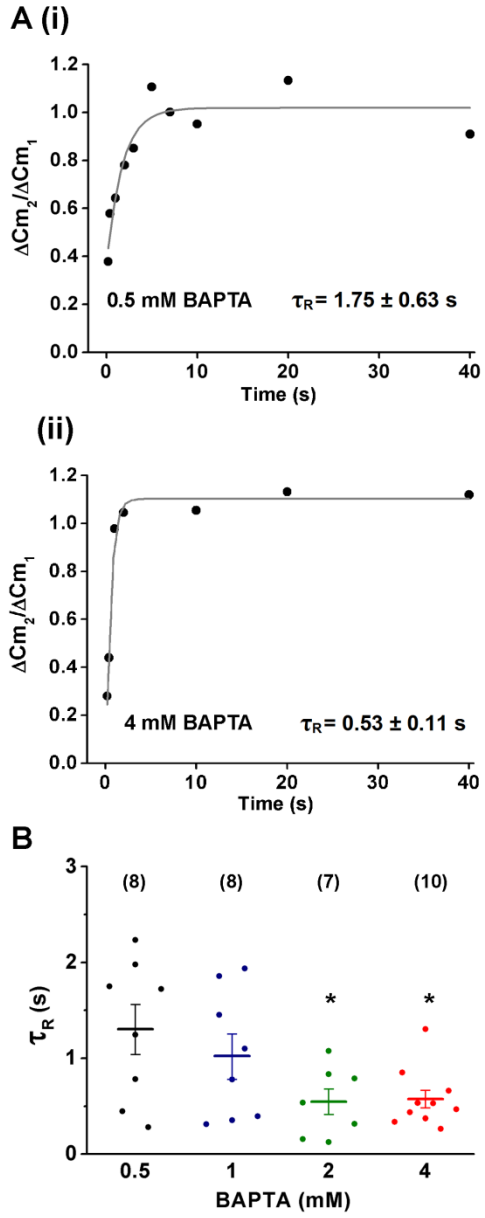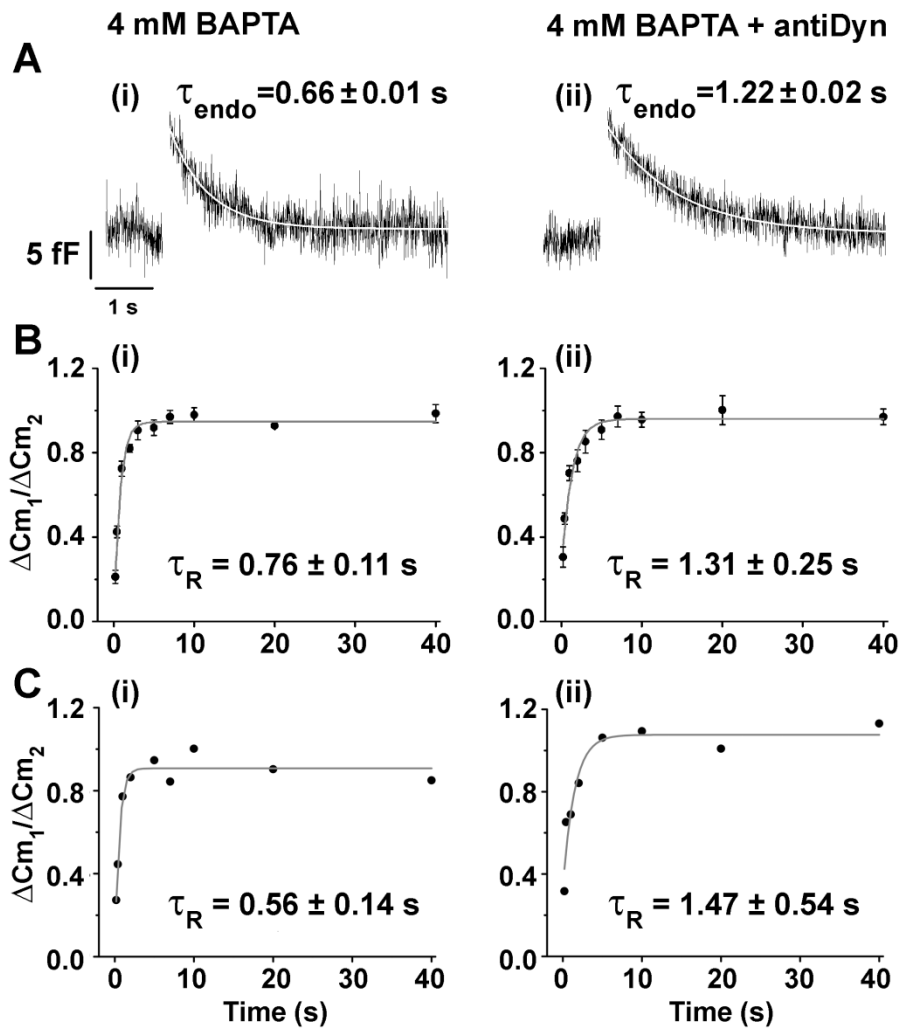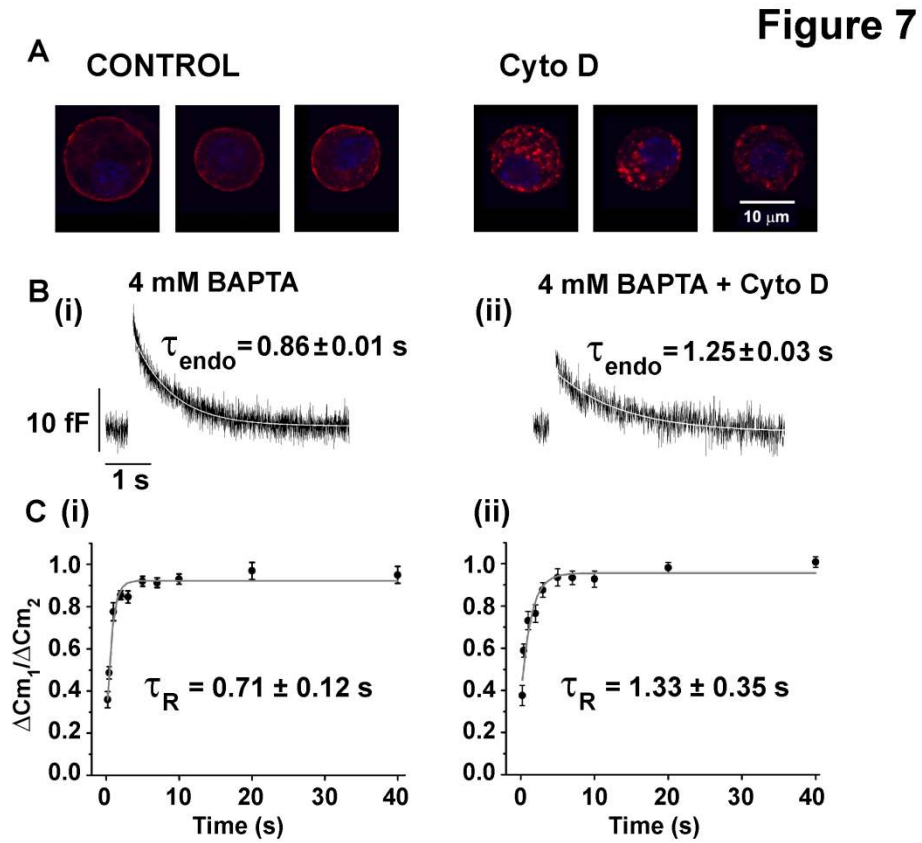
jnc_15276_f7.tif

Figure 8

jnc_15276_f8.tif